AGU PUBLICATIONS

JGR

Journal of Geophysical Research: Atmospheres

RESEARCH ARTICLE
10.1002/2016JD025161

Key Points:
- Existing frameworks relating variability in September Arctic sea ice extent to summer atmospheric circulation patterns have limitations
- Summer circulation patterns preceding large negative departures in September extent with respect to the linear trend are highly variable
- Summer circulation patterns preceding the large positive departures in September extent with respect to the trend are also highly variable

Correspondence to:
M. C. Serreze,
serreze@nsidc.org

Citation:
Serreze, M. C., J. Stroeve, A. P. Barrett, and L. N. Boisvert (2016), Summer atmospheric circulation anomalies over the Arctic Ocean and their influences on September sea ice extent: A cautionary tale, *J. Geophys. Res. Atmos.*, *121*, 11,463–11,485, doi:10.1002/2016JD025161.

Received 29 MAR 2016
Accepted 4 AUG 2016
Accepted article online 8 AUG 2016
Published online 10 OCT 2016

Summer atmospheric circulation anomalies over the Arctic Ocean and their influences on September sea ice extent: A cautionary tale

Mark C. Serreze[1], Julienne Stroeve[1], Andrew P. Barrett[1], and Linette N. Boisvert[2]

[1]National Snow and Ice Data Center, Cooperative Institute for Research in Environmental Sciences, University of Colorado Boulder, Boulder, Colorado, USA, [2]Earth System Science Interdisciplinary Center, University of Maryland, College Park, Maryland, USA

Abstract Numerous studies have addressed links between summer atmospheric circulation patterns and interannual variability and the downward trend in total September Arctic sea ice extent. In general, low extent is favored when the preceding summer is characterized by positive sea level pressure (SLP) anomalies over the central Arctic Ocean north of Alaska. High extent is favored when low pressure dominates. If such atmospheric patterns could be predicted several months out, these links provide an avenue for improved seasonal predictability of total September extent. We analyze detrended September extent time series (1979–2015), atmospheric reanalysis fields, ice age and motion, and Atmospheric Infrared Sounder data, to show that while there is merit to this summer circulation framework, it has limitations. Large departures in total September extent relative to the trend line are preceded by a wide range of summer circulation patterns. While patterns for the four years with the largest positive departures in September extent have below average SLP over the central Arctic Ocean, they differ markedly in the magnitude and location of pressure and air temperature anomalies. Differences in circulation for the four years with the largest negative departures are equally prominent. Circulation anomalies preceding Septembers with ice extent close to the trend also have a wide range of patterns. In turn, years (such as 2013 and 2014) with almost identical total September extent were preceded by very different summer circulation patterns. September ice conditions can also be strongly shaped by events as far back as the previous winter or spring.

1. Introduction

The pronounced decline in Arctic sea ice extent over the period of satellite observations has been a prominent topic in climate science and has garnered considerable attention by the media and general public. While there are downward linear trends in ice extent in all months [e.g., *Serreze et al.*, 2007], the decline is largest at the end of the melt season in September. The September trend over the period 1979–2015 of $-87100\,km^2\,yr^{-1}$ equates to −13.4% per decade as referenced to the mean September extent for the period 1981–2010 (Figure 1). The trend has arguably steepened over the past decade [*Serreze and Stroeve*, 2015]. It is expected that Arctic sea ice extent will continue to decline through the 21st century; the eventual outcome being an essentially seasonally ice free Arctic Ocean [*Stroeve et al.*, 2012a]. Ice loss is already having pronounced ecological impacts [*Post et al.*, 2013] and continued loss will make the Arctic more accessible to shipping, resource extraction, and other activities [*U.S. Navy*, 2014]. There is hence a need for better projections not only of the evolution of the sea ice cover on decadal and longer time scales but on seasonal time scales that bear directly on economic activities such as resource extraction and marine traffic.

Short-term seasonal predictability as well as decadal and longer-term projection is challenged by the high variability of ice extent about the long-term trend [e.g., *Kay et al.*, 2011; *Stroeve et al.*, 2014; 2015; *Swart et al.*, 2015]. *Serreze and Stroeve* [2015] highlight that year-to-year excursions in September extent exceeding $1.0\times10^6\,km^2$ are not uncommon in the satellite record (Figure 1). For example, the highest September extent of $7.88\times10^6\,km^2$ that occurred in 1996 was $1.75\times10^6\,km^2$ above the value for the previous year, 1995 (a relative increase of 28%). Extent then dropped by more than a million square kilometers between 1996 and 1997. The second lowest September extent of $4.30\times10^6\,km^2$, recorded in 2007, was $1.92\times10^6\,km^2$ below the 2006 value, a relative decrease of 45%. In turn, the record minimum extent of $3.63\times10^6\,km^2$ recorded in 2012 was followed in 2013 by a value of $5.35\times10^6\,km^2$, an increase of $1.72\times10^6\,km^2$ (nearly

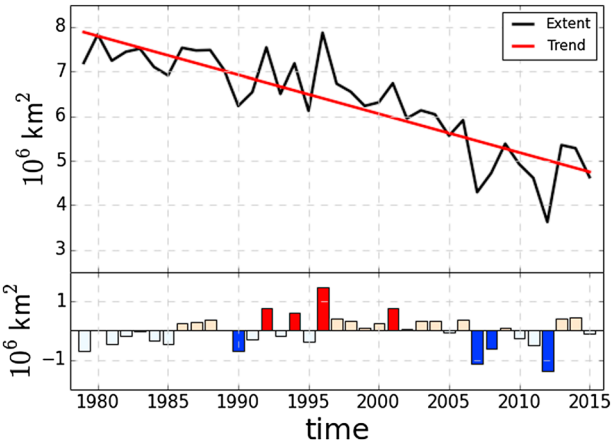

Figure 1. September sea ice extent over the period 1979–2015 with (top) linear trend line and (bottom) detrended anomalies, based on the combined satellite passive microwave record. The four years with the largest positive departures are shown in red (1992, 1994, 1996, and 2001); the four years with the largest departures (1990, 2007, 2008, and 2012) are shown in blue.

50%). Currently, seasonal forecasting systems are unable to forecast large departures from the trend line [*Stroeve et al*., 2014, 2015] at lead times of 1 to 6 months.

The large variability reflects both atmospheric and oceanic forcing. Atmospheric circulation variability has dynamic influences on the ice cover because the surface wind largely drives the sea ice circulation, affecting, for example, whether the ice motion is offshore or onshore, and the overall thickness distribution. Atmospheric circulation variability also has thermodynamic influences, manifested in factors such as ice melt and growth rates. The two components of atmospheric forcing often reinforce each other. For example, anomalous southerly winds may lead to offshore ice motion, leaving areas of open water along the coast, and also accentuate summer melt because southerly winds are also warm winds. Anticyclonic conditions favor clear skies, meaning more solar radiation at the surface, while cyclonic conditions tend to have the opposite effect. Ocean forcing includes heat transport into the Arctic from both the Pacific [e.g., *Shimada et al*., 2006; *Woodgate et al*., 2010] and the Atlantic [*Polyakov et al*., 2010; *Alexseev et al*., 2013]. *Onarheim et al*. [2015] have shown that Atlantic inflow is a strong predictor of sea ice variability in the Barents Sea. Atmospheric forcing and oceanic forcing are often tightly coupled, especially through summer heat uptake in the ocean mixed layer and its subsequent release through autumn and winter [e.g., *Jackson et al*., 2012; *Notz and Marotzke*, 2012].

Past studies have addressed atmospheric links in frameworks ranging from individual case studies [e.g., *Serreze et al*., 1995; *Stroeve et al*., 2012b] to the phase and strength of modes of atmospheric variability (teleconnections) including the Arctic Oscillation (AO) [*Rigor et al*., 2002; *Ogi and Wallace*, 2007], Pacific North American pattern (PNA) [*L'Heureux et al*., 2008], the Arctic Dipole (AD) anomaly [*Wang et al*., 2009], an index based on linear regression between July to September sea level pressure over the Arctic Ocean and the May minus September ice extent [*Ogi et al*., 2008] to an assessment of extratropical cyclone distributions and tracks [*Screen et al*., 2011]. Most attention has been paid to the summer season. The general conclusion is that low September sea ice extent tends to be favored when the summer atmospheric circulation features positive sea level pressure (SLP) anomalies over the central Arctic Ocean north of Alaska, especially when paired with negative anomalies along the coasts of northern Eurasia. This configuration, for which the summer of 2007 can be viewed as the exemplar (Figure 2) is associated with positive lower tropospheric (e.g., 925 hPa) temperature anomalies over much of the Arctic Ocean, negative anomalies in cloud cover (not shown), offshore ice motion along the eastern Eurasian coast, and a strong surface pressure gradient across Fram Strait, hastening sea ice transport out of the central Arctic Ocean through Fram Strait [*Stroeve et al*., 2008]. By contrast, Septembers with high sea ice extent show an association with negative SLP anomalies over the central Arctic Ocean, attended by negative temperature anomalies and reduced ice export out of Fram Strait. A good example is provided by the summer of 1996 (Figure 3), which preceded the highest September sea ice extent in the satellite record (see Figure 1). Broadly, this contrast in surface circulation can be related to the shape and strength of the summer 500 hPa circumpolar vortex. Summers with high SLP over the central Arctic Ocean occur when there is a strong 500 hPa ridge over the central Arctic Ocean, while low pressure dominates when the summer vortex is more symmetric, promoting the influx of low-pressure systems into the central Arctic Ocean [*Serreze and Barrett*, 2008; 2011]. There is evidence that the anticyclonic surface pattern has become more prominent in recent years [*Overland et al*., 2012], possibly linked to reduced spring snow over Eurasia [*Matsumura et al*., 2014].

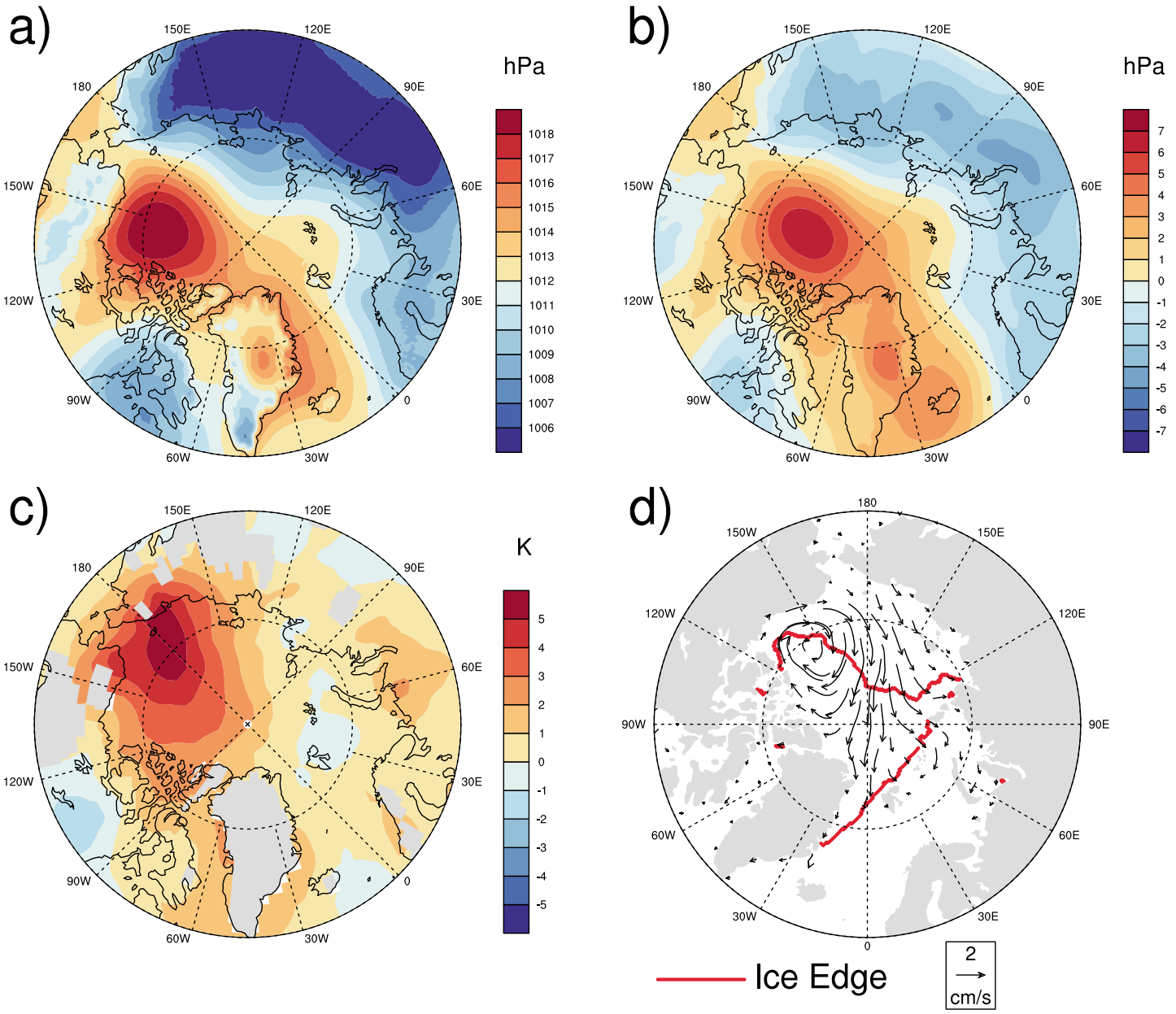

Figure 2. Fields of (a) sea level pressure, (b) sea level pressure anomalies, (c) 925 hPa temperature anomalies, and (d) mean ice velocity for the summer of 2007.

The objective of this paper is to demonstrate that while there is value in categorizing summer circulation patterns in terms of their influences on total September sea ice extent, there are strong limits to this framework. We show that different years with low September sea ice, taken as those with the largest negative departures in extent relative to the linear trend line, are preceded by sharp differences in summer circulation patterns, as are years with the largest positive departures in September sea ice extent relative to the trend line. Summer circulation patterns that precede Septembers with ice extent near the trend line are no less variable. In turn, one can identify years that, while having almost identical total September extent, were preceded by very different summer circulation patterns. While there are other important factors at work in addition to summer circulation, including aspects of ocean forcing, atmospheric forcing outside of the summer season, and spatial patterns of sea ice thickness, details of the location and magnitude of the summer circulation anomalies appear to be very important.

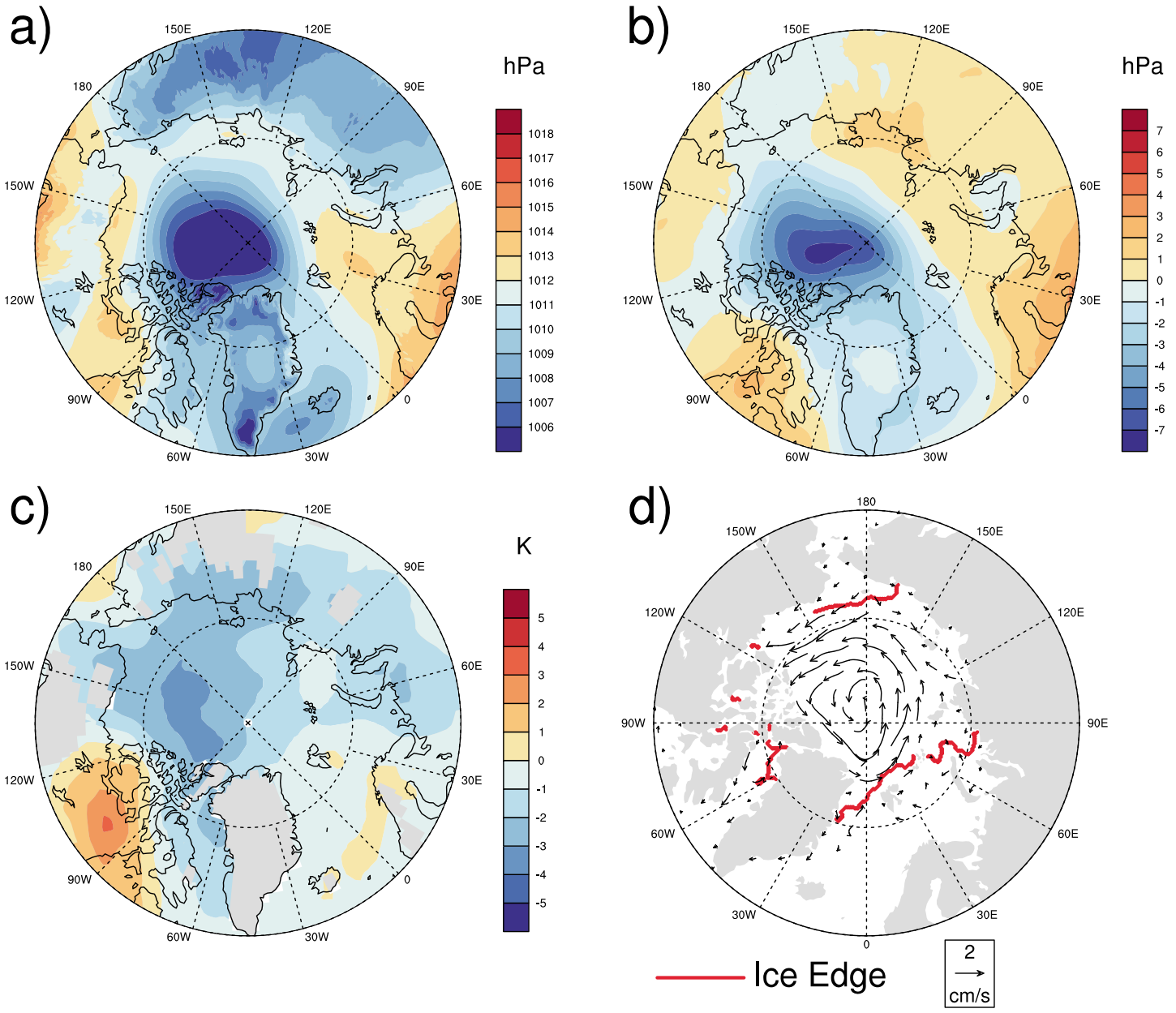

Figure 3. Fields of (a) sea level pressure, (b) sea level pressure anomalies, (c) 925 hPa temperature anomalies, and (d) mean ice velocity for the summer of 1996.

Our results argue that even if strong advances are made in providing general Arctic climate forecasts several months out, the use of such forecasts to improve predictability in September sea ice extent (either total extent or regional patterns) will be limited because the location of circulation anomalies would need to be accurately known. We adopt the standard definition of summer as the period June through August. While regional sea ice conditions can be influenced by individual events, such as strong storms [*Zhang et al.*, 2013], this choice provides consistency with many past studies, which in turn recognize that substantial regional anomalies in sea ice conditions are typically shaped by atmospheric anomalies over monthly to seasonal time scales [e.g., *Rogers*, 1978; *Serreze et al.*, 1995; *Ogi et al.*, 2008; *Wang et al.*, 2009]. However, we recognize that September ice conditions can also be strongly shaped by events as far back as the previous winter or spring, and even within a summer season, circulation can be highly variable. These issues are addressed as warranted in the discussion that follows. Determination of an optimal time frame for analysis of sea ice responses, while beyond the scope of the present study, stands out as a worthy research topic.

2. Data

2.1. MERRA

For analysis of atmospheric conditions, primary use is made of data from the Modern-Era Retrospective Analysis for Research and Applications (MERRA) reanalysis available for the period 1979–2015. Atmospheric reanalyses products like MERRA [*Rienecker et al*., 2011] represent retrospective forms of numerical weather prediction, using a fixed model and data assimilation system. Analyzed fields (analyses) such as of sea level pressure and geopotential heights, winds, temperature, and specific humidity at standard atmospheric levels represent the blending of a short-term atmospheric forecast with observations from radiosondes, satellite sounders, aircraft reports, and other sources. Each analysis cycle consists of collecting, selecting, and quality control of observations available within the analysis window; blending observations with a first guess of the state of the atmosphere (the short-term forecast) using a statistical interpolation scheme; and dynamically balancing the analysis and integrating the forecast model forward in time to the beginning of the next analysis cycle using the new analysis as initial conditions for the forecast step. The new forecast is used as the first guess for the next analysis cycle. Surface fields, such as of 2 m air temperature, precipitation, and surface fluxes, are generated as part of the forecast step. The MERRA analysis is performed at a horizontal resolution of 2/3° longitude by 1/2° latitude at 72 levels. Use is made of fields of SLP and temperature at the 925 hPa level (http://gmao.gsfc.nasa.gov/research/merra/). We prefer the 925 hPa temperature over the 2 m temperature because over a melting ice surface, the skin temperature is a constant regardless of energy inputs and there is hence little variability at the 2 m level. The 925 hPa temperature by contrast provides an indication of the thermal conditions in the lower troposphere. Other modern reanalyses include the National Oceanic and Atmospheric Administration Climate Forecast System Reanalysis (CFSR) and the Interim European Centre for Medium Range Weather Forecasting Re-Analysis (ERA-Interim). While outputs from different reanalyses are very similar with respect to analyzed fields in the troposphere, such as pressure heights and temperatures, they can differ strongly with respect to forecasted surface fields, such as precipitation, 2 m air temperature and surface radiation fluxes. *Jakobson et al*. [2012] undertook a comparison study for the central Arctic Ocean and found that ERA-Interim produces the most accurate profiles of humidity, temperature, and wind speed in the lower troposphere, while CFSR seems to perform the best with respect to surface flues. Our own analysis [*Serreze et al*., 2012] reveals that all reanalyses have warm and moist biases in the Arctic in the lowest atmospheric levels when compared to radiosonde data.

2.2. AIRS Products

To complement MERRA, use is made of products from the National Aeronautics and Space Administration (NASA) Atmospheric Infrared Sounder (AIRS). AIRS is a cross-track high spectral resolution infrared sounder on board NASA's Aqua satellite that was launched on 4 May 2002. AIRS collects radiance data with a 13.5 km spatial resolution in the horizontal at nadir and has 2378 infrared channels, from which geophysical products are generated dealing with the Earth and its atmosphere [*Ye et al*., 2007; *Susskind et al*., 2011, 2014; *Boisvert et al*., 2015]. AIRS has twice daily global coverage. The Level 3 data products used here are generated on a 1° by 1° latitude-longitude grid by including all Level 2-retrieved values in that grid box which have quality control flags representing retrievals thought to be of best or good quality. As case studies, we use monthly records for the years 2013 and 2014 of 1000 hPa geopotential height, 925 hPa air temperature, precipitable water (column water vapor), effective cloud fraction, and the turbulent sensible heat flux.

Retrieval steps are done sequentially and surface skin temperature, surface air temperature, and surface specific humidity are all derived independently of each other [*Susskind et al*., 2014]. Globally, roughly 80% of all retrievals at the surface are flagged as best or good quality in the version 6 data set used here. The AIRS retrieval process is unique in that it is able to measure surface properties under almost all sky conditions without the need of surface type classification [*Susskind et al*., 2003], whereas most satellite retrievals of surface products treat land, ocean, and sea ice surfaces differently and require classification of a scene for surface type and clear-cloudy sky prior to the retrieval. By doing this they create additional retrieval errors and also a bias toward clear-sky conditions.

The AIRS algorithm employs the cloud-clearing radiance approach iteratively within its retrieval algorithm such that the retrievals produce the best fit to the final cloud-cleared radiances. Using the nine 15 km hyperspectral IR measurements inside a 50 km multichannel microwave footprint, this technique takes advantage of cloud

inhomogeneity in a smooth clear-sky background to estimate what cloud-clear radiances should be as cloud fraction approaches zero, even where all nine infrared footprints are cloudy [*Susskind et al*., 2014].

Typically, cloud fraction is defined as the percentage of a pixel covered by clouds. However, AIRS produces an "effective cloud fraction," which is the radiative cloud fraction, representing the product of cloud amount and emissivity from infrared channels. Since it is not possible to separate emissivity from cloud amount, cloud fraction in the typical sense is not an AIRS product. In the infrared, cloud emissivity is a little less than 1.0; thus, the product of cloud fraction and emissivity is always lower than the true cloud fraction but still mimics typical visible cloud fraction products.

A known shortcoming of AIRS is gaps in the daily field variables where there is too much (or overly homogeneous) cloud cover in the field of view, obviating accurate retrievals. This problem is lessened by using monthly products. Using a variety of in situ data, *Boisvert et al*. [2015] found that skin temperature from AIRS were more accurate than in ERA-Interim, whereas the near-surface specific humidity was not as good. Other validation efforts, including assessment of turbulent fluxes, include *Tobin et al*. [2006], *Divakarla et al*. [2006], and *Dong et al*. [2010].

2.3. Sea Ice Extent

The satellite passive microwave record provides internally consistent estimates of Arctic sea ice extent from late 1978 through the present by combining data from the Nimbus 7 scanning multichannel microwave radiometer (SMMR, 1979–1987), the Defense Meteorological Satellite Program Special Sensor Microwave Imager (SSMI, 1987–2007), and the Special Sensor Microwave Imager/Sounder (SSMIS, 2008 to the present). While there are at least a dozen different sea ice algorithms that give sea ice concentrations and extent that are not necessarily consistent with each other, trends in the different data sets are generally consistent [*Ivanova et al*., 2014; 2015]. Here we use the monthly time series available from the National Snow and Ice Data Center (NSIDC) based on the NASA team algorithm [*Fetterer et al*., 2002] that has undergone extensive intersensor calibration to ensure consistency over the entire satellite data record. Accuracy of passive microwave retrievals depends on sea ice conditions, methods used in different validation studies as well as location. In general, winter retrievals of ice concentration from the NASA Team Algorithm are viewed as accurate to within ±5%, dropping to ±15% during summer because of melt ponds [*Cavalieri et al*., 1992]. Extent is defined as the area represented by all pixels with an ice concentration (fractional ice coverage) of at least 15%.

2.4. Sea Ice Motion Vectors and Ice Age

Fowler et al. [2004] showed that satellite and buoy data can be used to track individual sea ice parcels as they form, move on the Arctic Ocean surface, and disappear (through melt or transport out of the Arctic). The resulting daily resolution ice motion data set, available from NSIDC [*Fowler*, 2003] for the period 1979–2015 is based on ice motion vectors derived using a cross-correlation technique applied to sequential, daily satellite images acquired by the SMMR, SSMI, SSMIS, and advanced very high resolution radiometer sensors. The passive microwave imagery at 25 km resolution provides daily motions with an RMS accuracy of ~6–7 km/d when using oversampling techniques; 12.5 km resolution imagery (e.g., from the 91 GHz channel on SSMIS) can provide daily motions with an RMS accuracy of ~4–5 km/d. An Optimal Interpolation scheme takes advantage of the spatial correlation of neighboring motion estimates to create gridded fields with uncertainties of 3–4 km/d. While the RMS errors are fairly high, certainly when compared to average daily ice drifts that typically range between 5 and 15 km/d, there is little or no bias in the motion estimates. *Kwok et al*. [1998] compared ice motion estimated from ERS-1 synthetic aperture radar along with drifting buoy motion to the Lagrangian motion product and found an error of 5 to 12 km/d. However, this error is not necessarily cumulative, as annual displacement errors are on the order of 50–100 km. *Tschudi et al*. [2010] further evaluated the accuracy of the Lagrangian tracking. When an ice drift track was matched up with the drifting SHEBA ice camp, a displacement of only 27 km occurred over the period of 293 days. We use summer average motion vectors. Smoothing daily vectors over time (in our case, over summer seasons, as in Figures 2 and 3) reduces the RMS error.

Using the daily ice motion fields, *Fowler et al*. [2004] and *Maslanik et al*. [2007, 2011] developed an ice age data set by treating each grid cell that contains ice as an independent Lagrangian particle and advecting the particles at weekly time steps. Error in the Lagrangian tracking is dependent on spatial resolution,

geolocation and binning errors for each image pixel [*Meier et al*., 2000]. Atmospheric effects and temporal variability of the surface also introduce error, especially during summer. However, filtering techniques reduce these errors, and in many cases compensating errors reduce the net error in the parcel locations.

3. Analysis and Results

3.1. Overview

To set the stage, analysis starts with an assessment of spatial correlations between the detrended September ice extent time series (Figure 1) and detrended time series sea level pressure, temperature, relative vorticity, and winds. This is followed by a closer look at recent shifts in atmospheric circulation and temperature patterns. Attention then turns to individual years, looking at detrended spatial anomaly patterns of SLP and 925 hPa temperature associated with extreme negative and positive detrended anomalies in September sea ice extent, as well as for Septembers with extent near the line trend line. Finally, we examine two successive years (2013 and 2014) that ended up having almost the same September ice extent but were preceded by very different patterns of summer atmospheric circulation and temperature anomalies.

The detrended September sea ice time series was calculated by simply subtracting the value from the linear trend (estimated from least squares) for each year from the corresponding raw extent value. The September sea ice trend is viewed as the response to external forcing and the departures from the trend line as the internal variability. It is recognized that the trend may not be entirely forced as it may be affected by internal variability on decadal and even multidecadal scales [*Kay et al*., 2011]. It has been argued that the decline in September sea ice extent has steepened after about 1996 [e.g., *Serreze and Stroeve*, 2015]. If a second-order trend was applied to the September time series, then the years chosen as departing most strongly from the trend line (as well as those determined to be sitting close to the trend line) might change. However, no attempt has been made to utilize a second-order trend, the reason being that a linear trend is still the most defensible (i.e., conservative) model to adopt.

With respect to the atmospheric fields from MERRA, we linearly detrend at each MERRA grid point and for each variable. The primary concern is with respect to temperature anomalies. Although trends vary widely between region and by season, Arctic air temperatures are overall known to be rising. With a positive trend, temperature anomalies, if computed simply with respect to the long-term average, will tend to be negative in the early part of the time series and positive in the later part of the time series, which can mask signals related to atmospheric circulation. Using detrended anomalies helps to avoid this. The need to detrend other variables is less obvious, but it is done for completeness, and there are in fact trends in the sea level pressure fields (see section 3.2), which may contain a forced component.

3.2. Spatial Correlation Maps

Figure 4 shows spatial patterns of correlations between the detrended September sea ice extent over the period 1979–2015 and summer (June through August) detrended MERRA fields for each year of (a) sea level pressure, (b) 925 hPa temperature, (c) relative vorticity of the 10 m wind, and (d) the 1000 hPa meridional wind. Vorticity is calculated using the detrended 10 m wind components. The vorticity and wind fields are strongly influenced by topography, so for these variables the analysis is restricted to ocean regions. Correlation patterns computed with and without detrending the sea level pressure, temperature, and winds are very similar. None of the correlations shown in Figure 4 are strong (they are less than 0.4), and apart from the 925 hPa temperature, few appear to be significant at the 95% confidence interval. The correlation maps nevertheless capture relationships noted in previous studies.

For sea level pressure, the correlation pattern indicates that positive departures in September sea ice extent are favored when low pressure dominates the central Arctic Ocean and vice versa. This is consistent with both the correlation pattern of the 925 hPa temperature anomalies and of the relative vorticity of the 10 m wind. High (low) September extent with respect to the trend line is favored when 925 hPa temperatures over the Arctic Ocean are below (above) average. This makes sense as with cool conditions there will be less summer melt. This reflects changes in the polar vortex structure noted earlier—anticyclonic flow at the surface of the central Arctic Ocean is favored when there is a strong 500 hPa ridge over the region. When this ridge is weak or absent, the vortex is more symmetric, promoting the migration of cold-cored cyclones into the central Arctic Ocean [*Serreze and Barrett*, 2008; 2011; *Screen et al*., 2011]. As noted by *Screen et al*. [2011], this

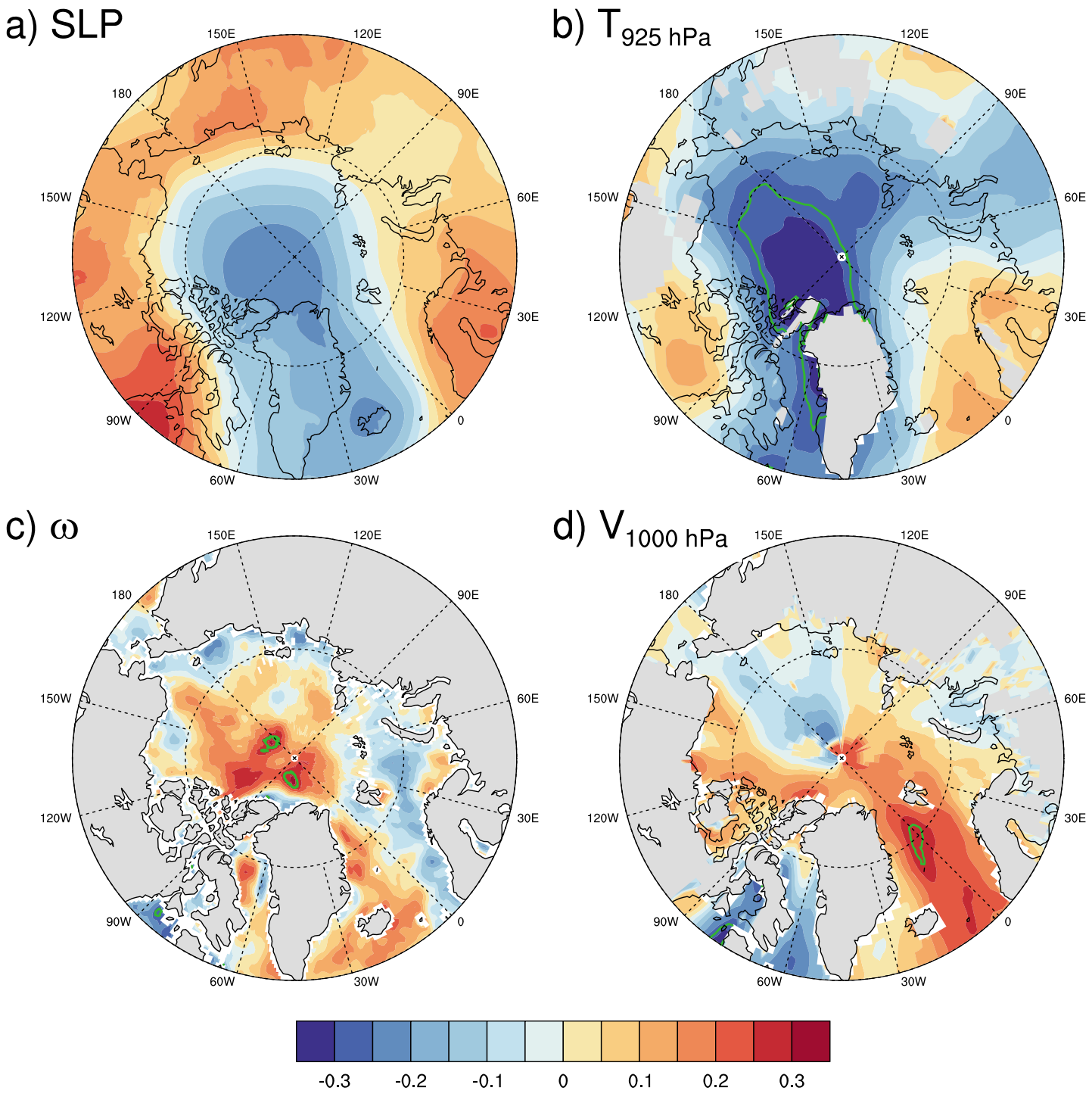

Figure 4. Spatial correlations between September sea ice extent and (a) sea level pressure, (b) 925 hPa air temperature, (c) 10 m wind relative vorticity, and (d) 1000 hPa meridional wind. Areas where the trends are statistically significant at the 95% level are enclosed by the green lines.

cyclone-associated precipitation may fall as snow, with the added effect of increasing the surface albedo. However, relationships are complicated in that strong cyclones also tend to break up the ice cover, allowing for enhanced absorption of solar radiation in open water areas [*Serreze et al.*, 2003; *Stroeve et al.*, 2005] and may also enhance melt through mixing, bringing warm water to the surface [*Zhang et al.*, 2013]. The positive (but again low) correlations with relative vorticity over the central Arctic Ocean show that low September sea ice extent is favored when the winds have an anomalous anticyclonic (negative relative vorticity) component

and vice versa for high extent. Dynamically, a more anticyclonic sea ice circulation in summer will tend to favor reduced extent because the ice motion will tend to be slightly convergent. *Ogi and Wallace* [2007] capture some of these relationships in the framework of the "summer Arctic Oscillation" (AO) mode of variability; this contrast is demonstrated by the sharply different circulation patterns for the summers of 2007 (positive summer AO) and 1996 (negative summer AO) (Figures 2 and 3).

Finally, note the positive correlations between September sea ice extent and the summer-averaged meridional (north-south) wind component on the Atlantic side of the Arctic along the longitudes corresponding to Fram Strait. This implies that positive anomalies in September extent tend to occur when the winds in Fram Strait have an anomalous component from south to north (positive anomaly), which will inhibit the export of ice out of the Arctic Ocean. Conversely, meridional winds in the region with an anomalous component from north to south (negative, down the strait, such as was clearly the case in summer 2007) are associated with negative anomalies in September extent. This relationship has also been noted in a number of past studies, such as *Wang et al*. [2009].

Interpretation of this statistical relationship, however, is not entirely intuitive. An additional correlation analysis reveals that a strong north to south wind through Fram Strait, while favoring the export of ice through Fram Strait, in turn favors positive anomalies in ice extent (or concentration) in the East Greenland Sea sector. For grid cells within and near the Fram Strait, these correlations are greater than 0.5, or roughly 25% of the variance of ice concentration in the East Greenland Sea. Given that the East Greenland Sea sector is typically (and as done here) included in the calculation of total Arctic sea ice extent, the thinking that the ice exported through Fram Strait simply exits the Arctic Ocean and melts away does not work. The correlation between ice concentration in the East Greenland Sea and for the remainder of the Arctic Ocean is actually quite low. What this argues is that in some situations, the ice melts in the East Greenland Sea to lower the total Arctic extent while in other situations, higher extent in the East Greenland Sea is countered by stronger reductions elsewhere in the Arctic.

While the correlations shown in Figure 4 are fairly weak, *Ogi et al*. [2008] obtained a correlation of 0.72 over the period 1979–2006 between the difference in May to September total ice extent and fairly simple sea level pressure index. At each grid cell poleward of 65°N, they regressed the time series of July-August-September mean sea level pressure against the time series of May minus September total ice extent. The index was obtained by then summing the cosine-weighted grid cell products of the summer pressure anomalies and the regression coefficients. This fairly strong correlation can be understood in that they incorporate the spatial pattern of the relationship between local sea level pressure and total ice extent into a single index value for each year. This contrasts with Figure 4 which simply shows the local correlation between September ice extent and winds (or vorticity). A second regression model that combined May multiyear ice fraction and the June through September mean sea level pressure explained about 60% of the variance in total May minus September ice extent over the period 1979–2006.

3.3. Temporal Shifts in Circulation Pattern

It has been argued that the anticyclonic pattern favoring low September sea ice extent has become more prominent in recent years [*Overland et al*., 2012]. The linear trend pattern of summer-averaged (June through August) SLP computed from MERRA data over the period 1979–2015 (Figure 5) does point to statistically significant increases north of the Canadian Arctic Archipelago and Alaska and for the region over and surrounding the Greenland Ice Sheet, attended by significant negative trends over northern Eurasia. The trend pattern broadly resembles the SLP anomaly pattern for the summer of 2007 (Figure 2). The sharp peak in the trend value over central Greenland shown in Figure 5 must be viewed with the strong caveat that it is difficult to adjust surface pressures over the high-elevation ice sheet to sea level.

To examine circulation changes more closely, Figure 6 shows anomalies in summer-averaged sea level pressure and 925 hPa temperature from MERRA for the first 6 years of the record (1979–1985), and then for the decades 1986–1995, 1996–2005, and 2006–2015. The common feature shared between the period 1979–1985, the 1986–1995 decade, and the 1996–2005 decade is modest negative SLP anomalies over the Canada Basin north of Alaska and the Canadian Arctic Archipelago. However, from a *t* test, these anomalies are not statistically significant. In the last decade (2006–2015) there is a clear shift to prominent and statistically significant positive anomalies in sea level pressures over the Canada Basin and Greenland. There is also a

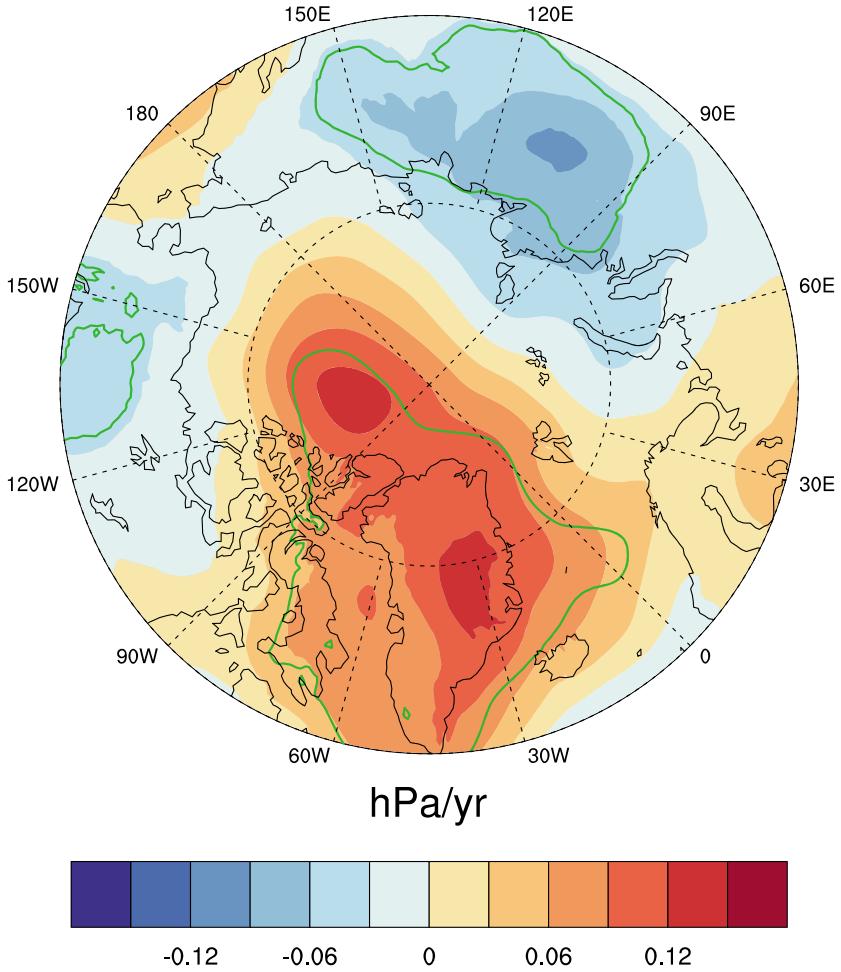

Figure 5. Linear trends in summer sea level pressure, 1979–2015. The areas where the trends are statistically significant are enclosed by heavy green lines.

shift toward negative anomalies over land areas (and toward stronger negative anomalies over north central Eurasia). These results hence indicate that while the linear trend pattern shown in Figure 5 primarily results from changes over the past 20 years, the most recent decade stands out strongly in comparison to the remainder of the record. Note also from Figure 6 the progression from largely negative 925 hPa temperature anomalies to positive anomalies for the most recent (2006–2015) decade.

3.4. Patterns for Individual Summers

Conclusions that one can (a) identify basic summertime atmospheric anomaly patterns linked to positive and negative departures in September ice extent relative to the trend line and that (b) there has been a shift in the average summer circulation over the past two decades favoring low September extent must be tempered by recognition of strong variability in summer patterns. As a start to illustrating this variability, we look at detrended sea level pressure and 925 hPa temperature anomaly patterns for the summers preceding the four Septembers with the largest negative departures in total ice extent relative to the trend line (1990, 2007, 2008, and 2012, Figure 7) and for the four Septembers with the largest positive departures in ice extent relative to the trend line (1992, 1994, 1996, and 2006, Figure 8).

There are arguably as many differences as there are similarities between the four years with the largest negative departures. Three of the four (2007, 2008, and 2012) feature positive pressure anomalies over and surrounding Greenland. Three of the four years also show a sea level pressure anomaly pattern giving rise to an enhanced pressure gradient across the Fram Strait (higher pressure to the west, lower pressure to the east), which has

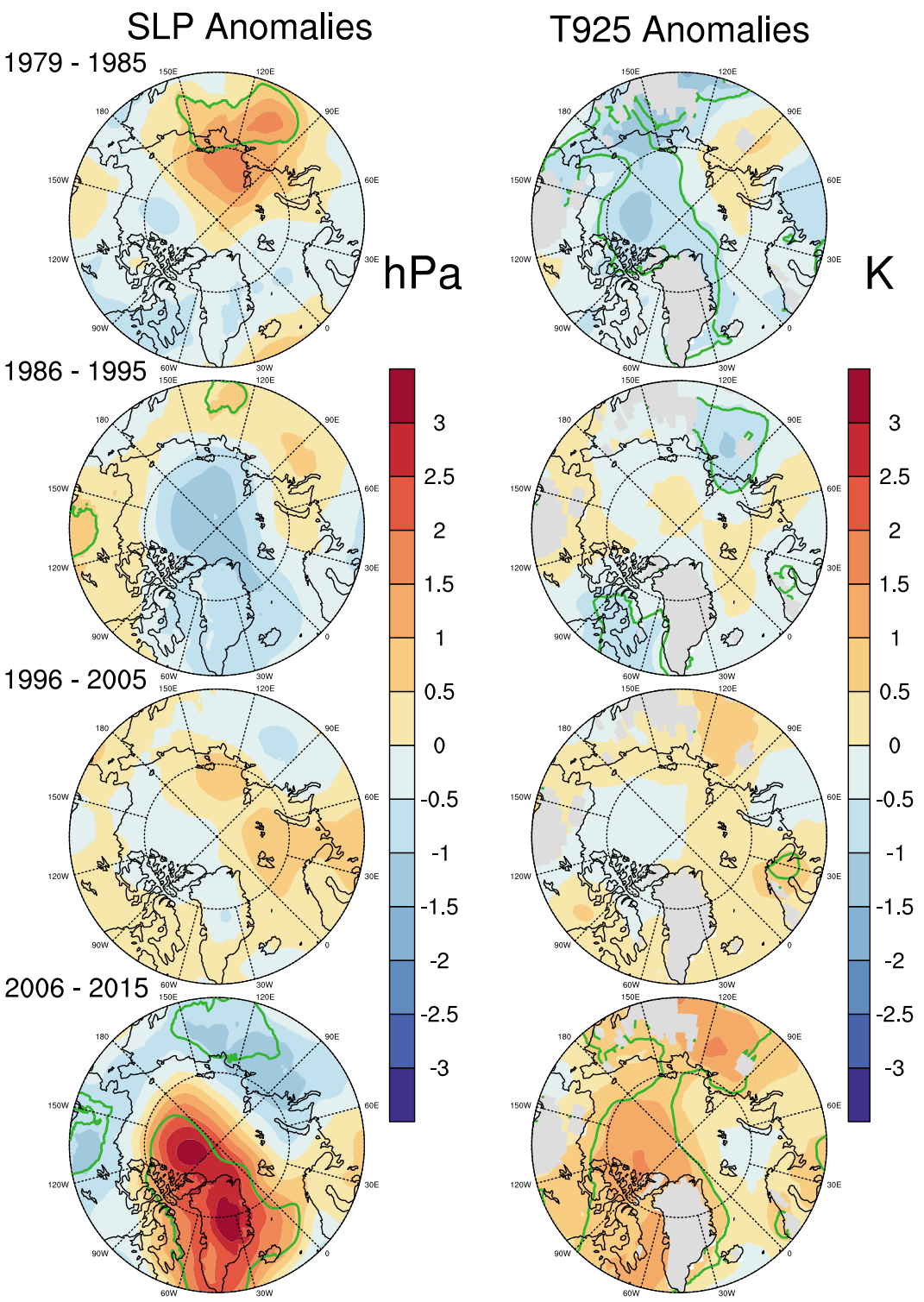

Figure 6. Summer anomalies of sea level pressure and 925 hPa temperature for 1979–1985 and for the decades 1986–1995, 1996–2005, and 2006–2015. Areas where the anomalies are statistically significant at the 95% level from a *t* test are enclosed by the green lines.

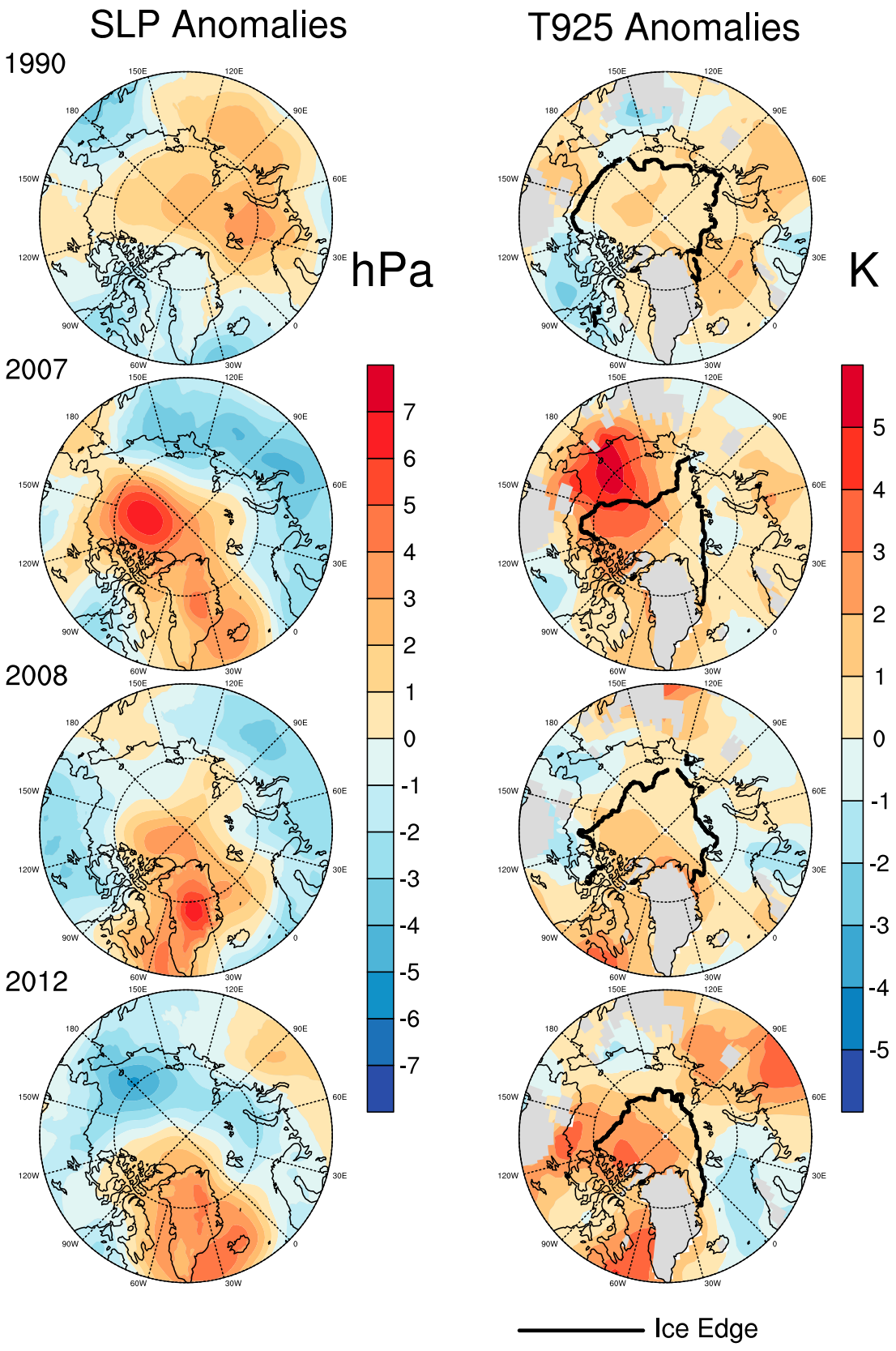

Figure 7. Summer sea level pressure and 925 hPa temperature anomaly patterns preceding the four Septembers with the largest negative departures in sea ice extent with respect to the linear trend line (see Figure 1), along with the spatial patterns of September ice extent.

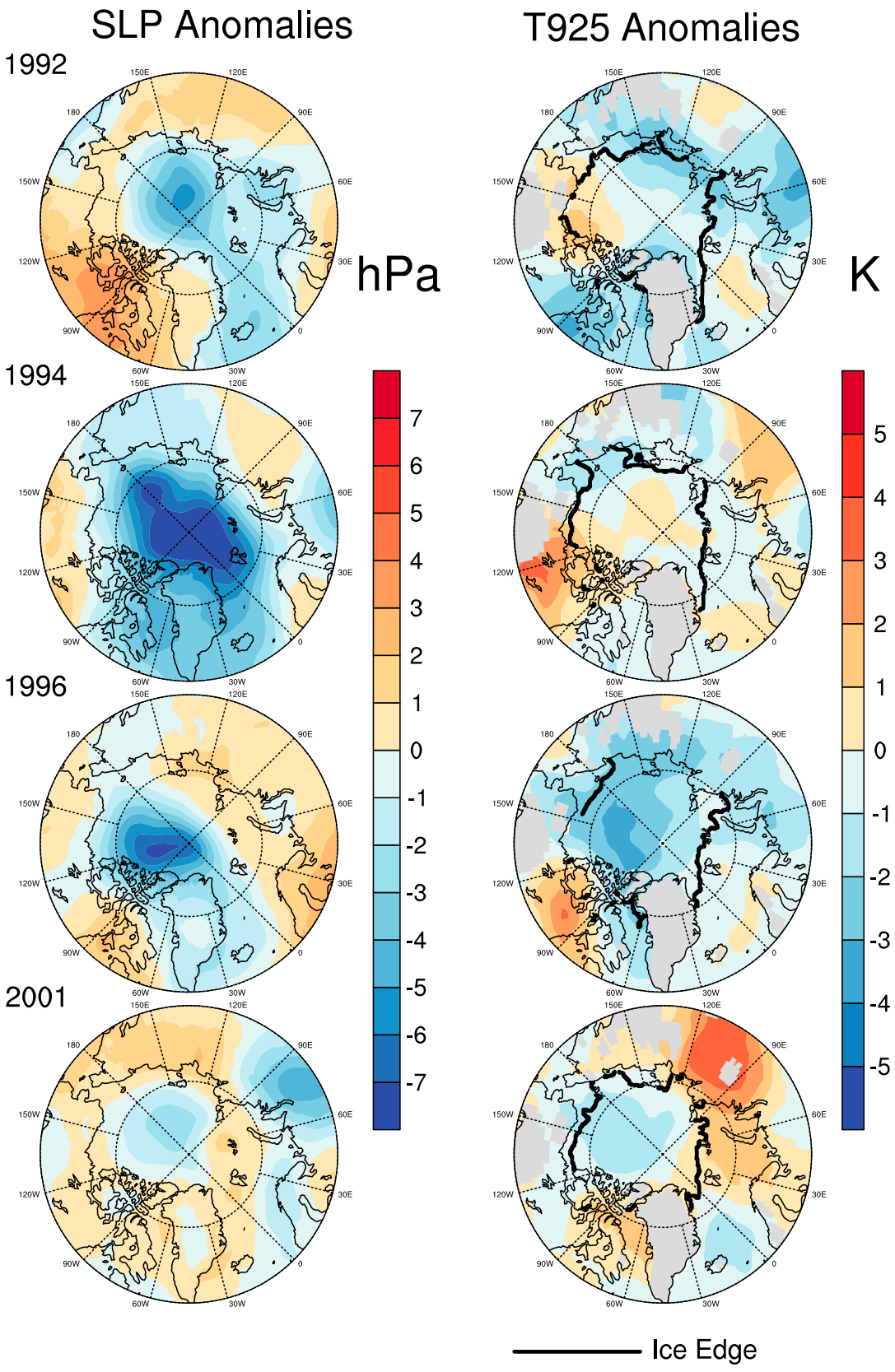

Figure 8. Summer sea level pressure and 925 hPa temperature anomaly patterns preceding the four Septembers with the largest positive departures in sea ice extent with respect to the linear trend line (see Figure 1), along with spatial patterns of September ice extent.

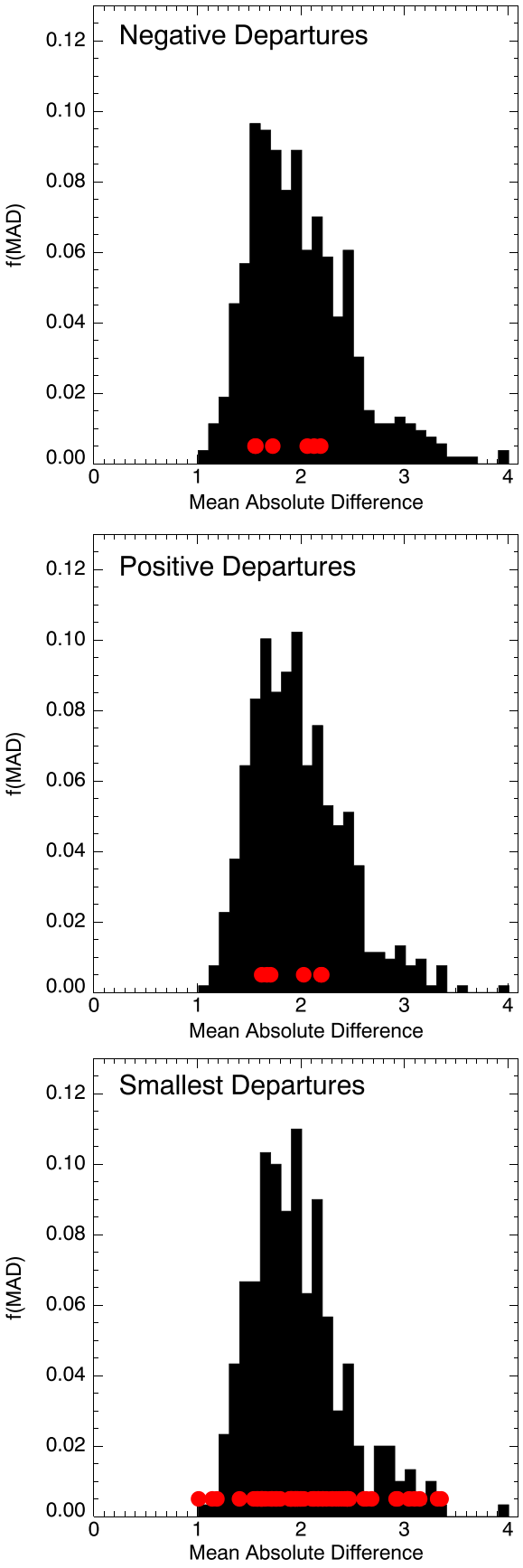

long been recognized as favoring sea ice export into the East Greenland Sea [e.g., *Vinje and Finnekasa*, 1986]. However, the pattern for 1990, with positive SLP anomalies centered over the Barents Sea, would have instead worked to reduce the Fram Strait flux. While for both 2007 and 2008, pressures were below average over northern Eurasia, in the summer of 2012 there was instead a region of negative anomalies lying further to the north, extending along the Eurasian coastal seas, most pronounced in the Chukchi and East Siberian seas. In 1990, pressure anomalies over northern Eurasia were slightly positive. Of all the years, only 2007 had a prominent positive pressure anomaly over the central Arctic Ocean. Turning to 925 hPa temperatures, while a common thread between the four years over the Arctic Ocean is the dominance of positive or neutral anomalies over negative ones, the spatial structure of anomalies was quite different.

As a quantitative evaluation, the similarity in SLP anomaly patterns between the four years with the largest negative anomalies in September ice extent was evaluated through the mean absolute difference between each pair of these years (1990 and 2007, 1990 and 2008, 1990 and 2012, 2007 and 2008, 2007 and 2012, and 2008 and 2012). This was done by simply taking the mean of the absolute differences between the SLP anomalies at each grid point for each pair. The grid point anomalies were first cosine weighted to account for convergence of the meridians. The

Figure 9. Frequency distribution of the mean absolute difference in summer sea level pressure anomalies based on (top) the pairs of years (red dots) with the largest negative anomalies in September sea ice extent with respect to the trend line and the remaining pairs of years, (middle) the pairs of years (red dots) with the largest positive anomalies in September sea ice extent with respect to the trend line and for the remaining pairs of years, and (bottom) the pairs of years (red dots) with anomalies in September sea ice extent within 250,000 km^2 of the trend line and for the remaining pairs of years.

same procedure was then applied to all of the pairs of the remaining years 33 years in the 1979–2015 record. Figure 9 (top) shows the frequency distribution of the mean absolute difference (MAD) for all pairs of years, with the MAD for the pairs of years with the largest negative sea ice departures shown by the red dots. If these pairs of years had SLP anomaly patterns that were more similar than the other pairs, they would be expected to cluster on the left side of the frequency distribution (small MAD), but they do not.

Not surprisingly, there are sharp differences between the four years in the spatial pattern of September sea ice extent. The link between summer atmospheric circulation and the September extent pattern for 2007 is fairly straightforward; extensive open water in the longitudes corresponding to the Chukchi and East Siberian seas reflects the strong positive summer temperature anomalies in these sectors, consistent with southerly wind anomalies that also promoted offshore ice motion from the eastern Eurasian coast. The temperature and pressure anomaly pattern for summer 2012 is in turn consistent with September of this year having more open water north of Alaska compared to 2007.

The circulation pattern preceding the low September sea ice recorded in 1990 is of particular interest. This year was previously examined by *Serreze et al*. [1995] as a case study. They found that over the May–June period, positive air temperature anomalies covered most of the Arctic Ocean, largest along the Siberian coast where early melt was observed and where open water at the end of the melt season in September was most extensive. This temperature anomaly pattern and early melt was attributed to a deep, mean low in the May pressure field (996 hPa; anomalies peaking at −20 hPa) centered at about 80°N,100°E, resulting in strong southerly winds along the Siberian coast and the early development of open water and low ice concentration in the Laptev and East Siberian seas. The open water anomaly, already large by July, grew rapidly during August, attributed to the development of a strong anticyclone located north of Alaska. This promoted easterly winds in the Chukchi and East Siberian Seas. Since the ice motion tends to be to the right of the geostrophic wind, this resulted in a poleward motion of ice away from the coast. In summary, the low September sea ice extent for 1990 appears to have been as much a result of the late spring atmospheric circulation as it was the late summer (August) circulation, neither of which are reflected in the summer average circulation field. Aspects of the winter circulation may have also played a role. Of note is that the period January through April of 1990 was characterized by a strongly positive phase of the winter Arctic Oscillation pattern. Statistically, such a pattern favors offshore ice motion from the Siberian coast, leaving areas of open water that refreeze, resulting in a fairly thin ice cover at the start of the melt season. This ice cover is more prone to melting out in summer [*Rigor et al*., 2002].

All four of the Septembers with sea ice extent strongly above the linear trend line (Figure 8) were associated with a summer circulation featuring negative pressure anomalies over the Arctic Ocean. So in this sense there is more similarity between the patterns associated with heavy ice years than there is for the years with low ice extent. Nevertheless, they again differ markedly in terms of the location and magnitude of the circulation and temperature anomalies, and the lack of overall similarity is evident after applying the same MAD analysis as employed for the low sea ice years (Figure 9, middle). For 1994, despite the strong negative sea level pressure anomalies, temperature anomalies over most of the Arctic Ocean were rather small. This argues that the high September extent for this year was largely determined by the ice motion. Only for 1996 (which as we recall had the highest September ice extent in the satellite record) does the pressure anomaly pattern point to a weaker than normal pressure gradient across Fram Strait; this would have worked in tandem with the cool conditions to limit sea ice loss (see also Figure 2). Again note the regional differences in September ice extent.

It is also instructive to examine detrended summer anomaly patterns in circulation for years that September ice extent ended up near (taken here as within 250,000 km^2 of) the linear trend line. It might be thought that such summers would be characterized by only modest anomalies in circulation patterns. As seen in Figure 10, this is obviously not the case. Indeed, the anomaly magnitudes are just as large as those shown in Figures 7 and 8 for extremely high and low ice years relative to the trend line, and the MAD analysis shows that a few of these years are quite similar to each other (Figure 9, bottom). One can also identify summers that the circulation pattern arguably should have favored a September extent well below the trend line (2009) or well above the trend line (1989). Consider in turn the contrast between 2002 and 2009. While these two summers differed sharply in terms of SLP anomaly patterns, September ice extent for both years ended up near the linear trend line (2009 slightly above and 2002 slightly below). Selecting years that fall close to a trend line determined using a nonlinear Locally Weighted Scatterplot Smoothing fit yields similar results.

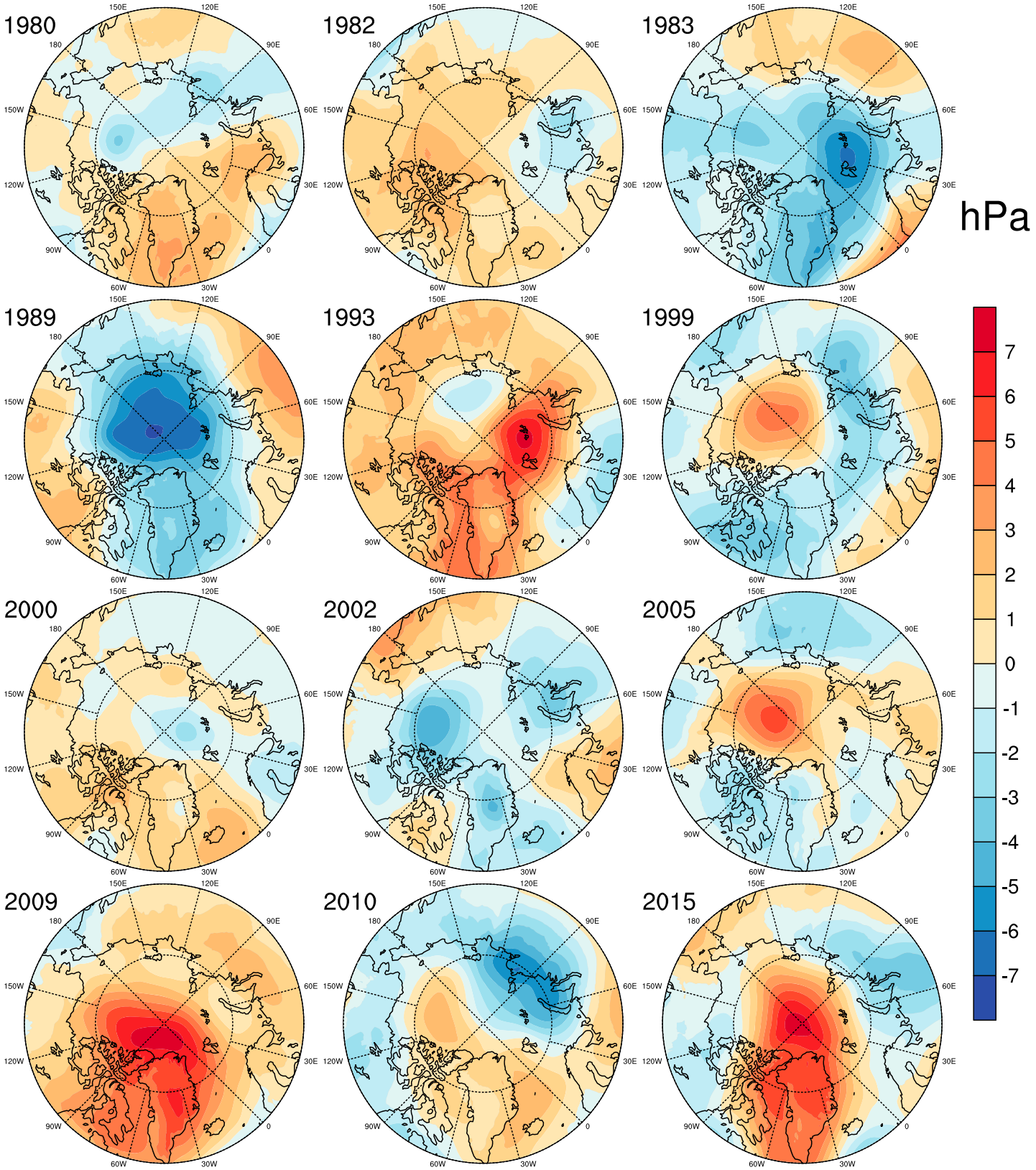

Figure 10. Summer sea level pressure anomaly patterns preceding the Septembers with sea ice extent within 250,000 km^2 of the linear trend line.

3.5. Detailed Case Studies

Sea ice and atmospheric conditions for 2013 and 2014 are examined as detailed case studies. We choose these two years because (a) in being subsequent years, comparisons can be very direct because there is no need to detrend the data; (b) September average sea ice extent was very similar for the two years, 5.35×10^6 km^2 and 5.28×10^6 km^2, respectively; the difference in extent between the two years is the smallest since 2000, and the third smallest difference since the sea ice record began; (c) patterns of atmospheric circulation were very different between the two years; and (d) the AIRS record can be used to examine atmospheric conditions in detail. We ask the question: Why was total September extent so similar for the two years despite such different patterns of summer circulation?

Figure 11 shows, for each year, the spatial distribution of April sea ice age, the summer-averaged pattern of ice motion vectors and September ice extent. The red lines show the median September ice edge calculated over the period 1979–2014. Compared to September 2013, the ice margin for September of 2014 lies further to the north in the longitudes corresponding to the Laptev Sea (marked as "L"). By contrast, the ice edge for September of 2014 lies further to the south in the Barents Sea sector (marked as "B"). The spatial pattern of April ice age is similar for the two years; the major difference is in the Beaufort Sea, where in 2014, ice of two years and older (multiyear ice) extended southward to the Alaskan coast. It is apparent that some of this coastal multiyear ice melted out in the summer of 2014 although some of it may have been moved away from the Arctic coast and into the central Arctic Ocean. The pattern of ice motion anomalies was quite different between the two years.

The contrasting regional anomalies in extent and ice motion can be understood in large part by looking at the summer-averaged anomaly from AIRS of 1000 hPa height, 925 hPa air temperature, and precipitable water along with the effective cloud fraction and turbulent sensible heat flux (Figure 12). The less extensive September ice for 2014 along the longitudes corresponding to the Laptev Sea is consistent with the pairing of positive 1000 hPa anomalies centered north of the East Siberian Sea and negative anomalies centered over the western Laptev Sea; winds between the two height anomaly centers had an anomalous component from the south, which as seen in Figure 11 helped to advect the ice offshore. This wind pattern is also consistent with the positive 925 hPa temperature anomalies in this area that would have promoted melt. The central Arctic Ocean in summer of 2013 was by contrast dominated by fairly strong negative anomalies in 1000 hPa height, associated with negative 925 hPa temperature anomalies. Based on the general relationships discussed earlier, this pattern would favor a positive departure in the detrended September ice extent. That the positive departure was rather small (and almost identical to that observed in 2014) likely relates to the wind-driven pattern of ice motion anomalies in the Barents Sea sector (Figure 11), tending to limit the usual southward advection of ice in this sector.

As would be expected, the summer anomaly patterns in precipitable water for the two years closely follow the air temperature anomaly patterns. While warmer air can carry more water vapor, more water vapor will tend to increase the downward longwave radiation flux (and vice versa). This may have contributed to the reduced ice extent in the Laptev Sea sector in 2014 compared to 2013. The role of cloud cover is less straightforward. One notable difference between the two years is that in 2013, positive anomalies (5–10%) in effective cloud fraction encompass a broad area including the Chukchi and Beaufort Seas, the Canadian Arctic Archipelago, and the region surrounding the North Pole. At issue is the direction of the total cloud radiative effect. For most of the year Arctic cloud cover has a warming effect at the surface (the increase in the downward longwave radiation flux exceeds the decrease in the downward shortwave flux). It may be negative for only a short time during summer. Note that the areas of positive summer cloud fraction anomalies for 2013 are also those with negative air temperature anomalies, implying either that the total cloud radiative effect was negative (cooling) or, if positive, was of small magnitude. We show the mean fields of the turbulent sensible heat flux as opposed to anomalies because the sign of anomalies depends on the sign of the flux itself (taken as positive downward, as a heat source to the surface, and negative upwards). The only notable difference between the two years is stronger upward fluxes (cooling the surface) over the central Arctic Ocean in 2013. This is qualitatively consistent with the cooler conditions in the area in 2013, pointing to less frequent surface melt and more frequent episodes with temperatures decreasing from the surface upwards. Not shown is the pattern of the turbulent latent heat flux—differences between the two years are everywhere small over the Arctic Ocean.

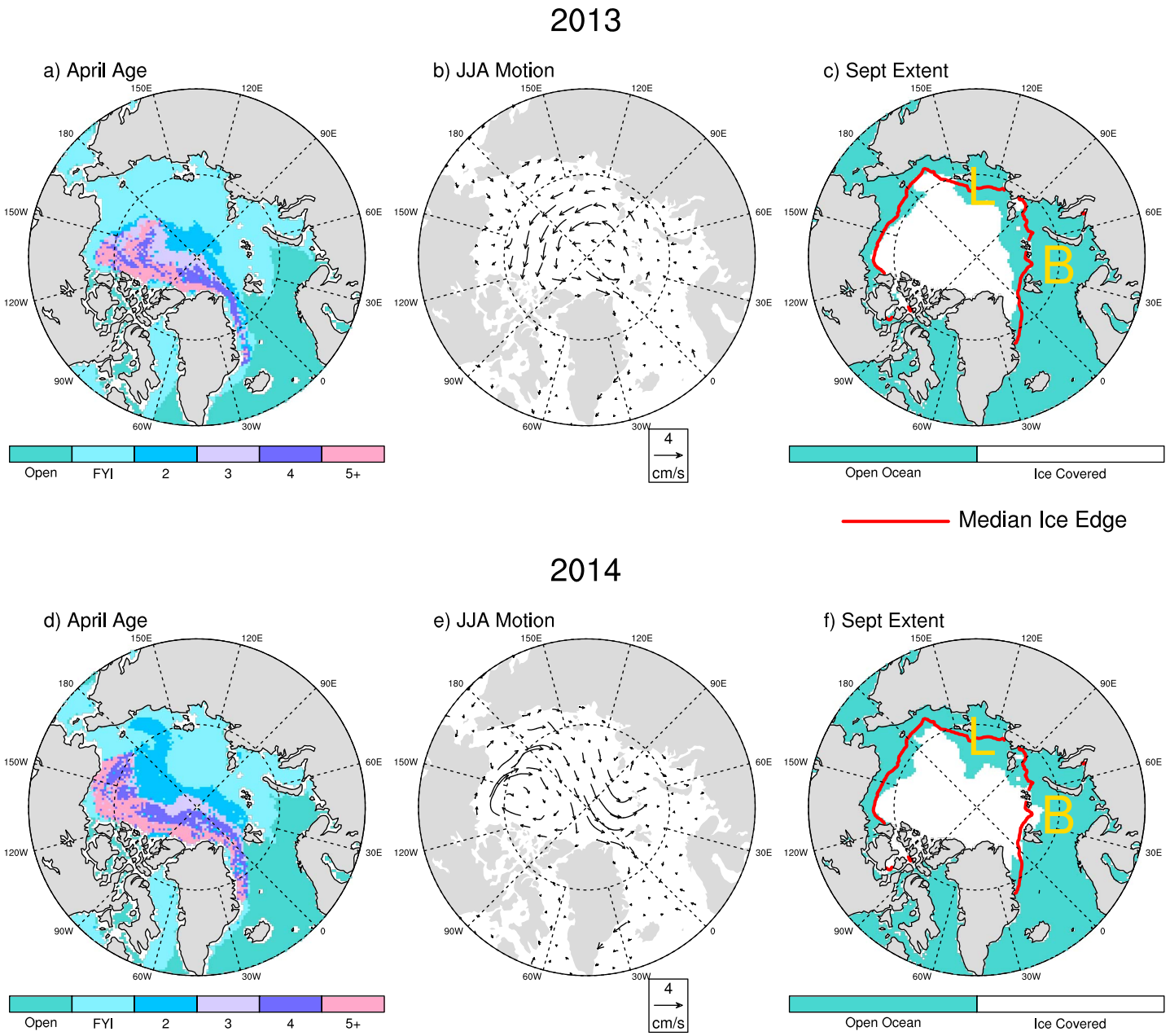

Figure 11. September ice age, summer-averaged ice motion vectors and September sea ice extent for 2013 and 2014. The red lines on the ice extent maps show the mean location of the ice edge over the period of record 1979–2015. The labels L and B identify the Laptev and Barents Sea sectors, respectively, which are referred to in the text.

4. Summary and Discussion

Key findings are summarized as follows:

1. Consistent with results from past studies, years with low (high) September sea ice extent, evaluated in terms of departures from the linear trend line, are favored by a summer atmospheric pattern promoting anticyclonic (cyclonic) surface wind anomalies over the central Arctic Ocean and winds with a stronger (weaker) than average component down Fram Strait. These two features were especially well expressed in the summer of 2007. Based on correlation analyses, these general relationships are fairly weak. Having said this, *Ogi et al.* [2008] were able to find a fairly strong correlation between the May to

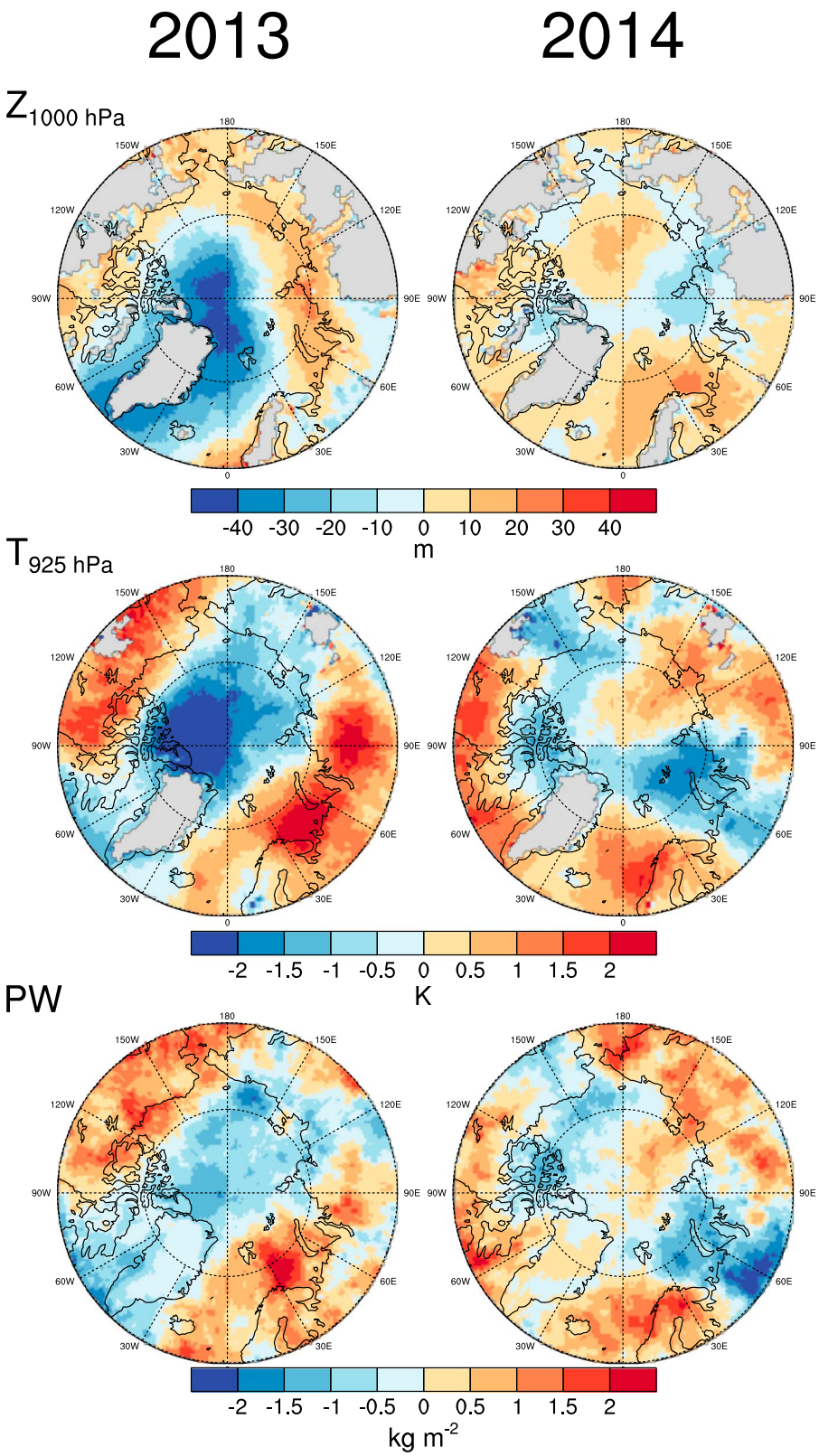

Figure 12. Summer-averaged anomalies in (a) 1000 hPa height, 925 hPa temperature, and precipitable water, and (b) effective cloud fraction anomalies and the turbulent sensible heat flux for the years 2013 and 2014 based on AIRS data. Anomalies are computed with respect to the period 2003–2015 covered by AIRS. The sensible heat flux is not shown as an anomaly because the sign of anomalies depends on the sign of the flux itself (positive downward).

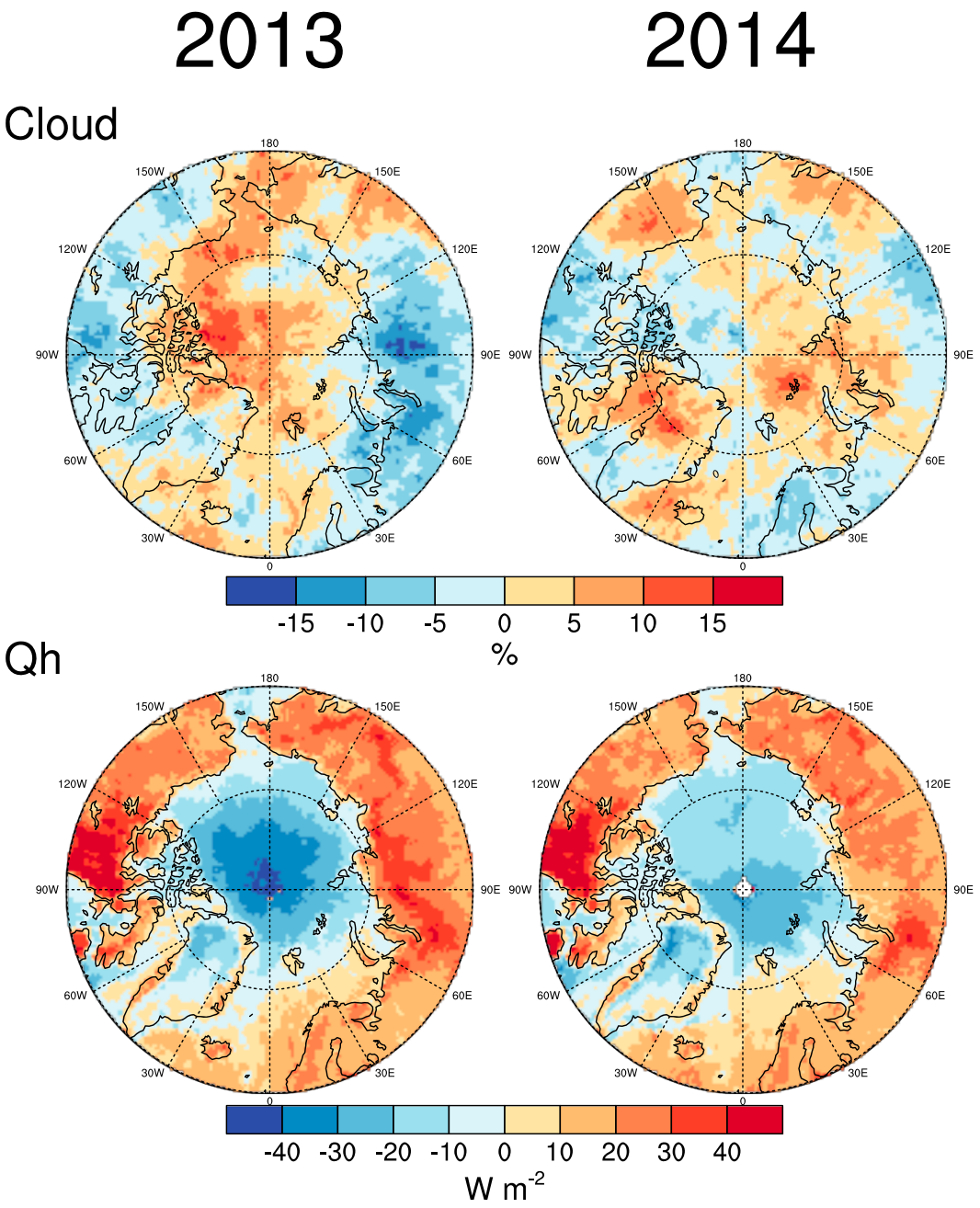

Figure 12. (contiued)

September difference in ice extent and an index that incorporates the spatial pattern of the relationship between local sea level pressure and the May to September extent difference.

2. Also consistent with previous studies, there has been a shift over the past 20 years toward summer sea level pressure patterns favoring summer ice loss. This shift is characterized by increases in sea level pressure north of Alaska and the Canadian Arctic Archipelago and over and around Greenland, coupled with decreases in pressure over northern Eurasia.
3. While summer circulation anomalies that precede years with the largest negative departures in September ice extent with respect to the linear trend line are broadly consistent with expectations, there are marked differences between each case. The same holds for the years with the largest positive departures in September ice extent with respect to the linear trend line.

4. Summer atmospheric circulation anomalies for years preceding Septembers with ice extent close to (within 250,000 km^2) of the trend line are highly variable; one can identify summers for which the circulation pattern arguably should have favored a September extent well below the trend line or well above the trend line. In turn, one can identify patterns that arguably should have led to very different departures in total extent from the trend line but did not.
5. The argument that a wind pattern favoring a strong Fram Strait ice flux is associated with low September sea ice extent is an oversimplification—such a wind pattern actually favors more ice in the East Greenland Sea. One explanation is that despite the higher extent in the East Greenland Sea, enough of the ice still melts in the region to yield a lower total Arctic extent. It may also be that a higher extent in the East Greenland Sea is countered by stronger reductions elsewhere in the Arctic.

We reiterate that while the examination of years relative to the linear trend in September extent helps to separate the ice response to atmospheric forcing from the externally forced response, it cannot completely account for changes in the character of the sea ice cover, notably thickness, which may change the response of ice extent to a given atmospheric forcing.

We also stress that a focus on the summer season, widely adopted in prior studies, is inadequate. As just one example, while September ice extent for 1990 was well above the trend line, it appears that atmospheric forcing the preceding winter and spring was at least as important as what happened in summer [*Serreze et al*., 1995; *Rigor et al*., 2002]. This points to the need for research on optimal time windows for studying sea ice responses to atmospheric forcing. We have also not considered ocean forcing in our study, which is increasingly recognized as important in September sea ice variability and the downward trends [*Shimada et al*., 2006; *Polyakov et al*., 2010; *Woodgate et al*., 2010; *Jackson et al*., 2012; *Notz and Marotzke*, 2012; *Alexseev et al*., 2013].

All of these factors contribute to the observation that similar summer atmospheric anomaly patterns can be followed by a wide range of September sea ice extent and that very different patterns can result in similar total extent. However, it also appears that even fairly minor differences in the location and strength of summer atmospheric circulation anomalies can lead to very different patterns of sea ice drift and air temperature anomalies. A sobering conclusion is that even if strong advances were made in providing general Arctic climate forecasts several months out, the use of such forecasts to improve predictability in September sea ice extent will be limited because the location of circulation anomalies would need to be accurately known.

The focus on total Arctic ice extent in this paper is in keeping the focus of much of the recent literature as well as community efforts such as the Sea Ice Prediction Network (https://www.arcus.org/sipn) and stems in large part from considering sea ice variability and trends from a climate point of view. However, it is important to note that as the Arctic becomes more accessible, more attention will need to be paid to predictability at the regional scale that has direct applications to shipping operations and other activities.

Acknowledgments

This study was supported by NSF grants PLR 1417016 and PLR130424 and by the Earth System Science Interdisciplinary Center (ESSIC) Task 683. Sea ice extent and other products used in this study are available from the National Snow and Ice Data Center (https://nsidc.org). The MERRA data can be downloaded from http://gmao.gsfc.nasa.gov/research/merra/. The monthly Bering Strait inflow data were provided by Rebecca Woodgate (University of Washington, Seattle); data can also be obtained at http://psc.apl.washington.edu/HLD/Bstrait/bstrait.html.

References

Alexseev, V. A., V. V. Ivanov, R. L. Kwok, and L. H. Smedsrud (2013), North Atlantic warming and declining volume of Arctic sea ice, *Cryosphere Discuss.*, *7*, 245–265, doi:10.5194/tcd-7-245-2013.

Boisvert, L. N., D. L. Wu, T. Vihma, and J. Susskind (2015), Verification of air/surface humidity differences from AIRS and ERA-Interim in support of turbulent flux estimation in the Arctic, *J. Geophys. Res. Atmos.*, *120*, 945–963, doi:10.1002/2014JD021666.

Cavalieri, D. J., et al. (1992), NASA Sea Ice Validation Program for the Defense Meteorological Satellite Program Special Sensor Microwave/Imager: Fonal report, NASA Tech. Memo. 104559, 126 pp. [Available at http://ntrs.nasa.gov/archive/nasa/casi.ntrs.nasa.gov/19920015007.pdf.]

Divakarla, M. G., C. D. Barnet, M. D. Goldberg, L. M. McMillin, E. Maddy, W. Wolf, L. Zhou, and X. Liu (2006), Validation of Atmospheric Infrared Sounder temperature and water vapor retrievals with matched radiosonde measurements and forecasts, *J. Geophys. Res.*, *111*, D09S15, doi:10.1029/2005JD006116.

Dong, S., S. T. Gille, J. Sprintall, and E. J. Fetzer (2010), Assessing the potential of the Atmospheric Infrared Sounder (AIRS) surface temperature and specific humidity in turbulent heat flux estimates in the Southern Ocean, *J. Geophys. Res.*, *115*, C05013, doi:10.1029/2009JC005542.

Fetterer, F., K. Knowles, W. Meier, and M. Savoie (2002), *Sea Ice Index, Digital Media*, Natl. Snow and Ice Data Cent., Boulder, Colo.

Fowler, C. (2003), *Polar Pathfinder Daily 25 km EASE-Grid Sea Ice Motion Vectors*, Natl. Snow and Ice Data Cent., Boulder, Colo. [Available at http://nsidc.org/data/nsidc-0116.html], (updated 2007).

Fowler, C., W. J. Emery, and J. Maslanik (2004), Satellite-derived evolution of Arctic sea ice age: October 1978 to March 2003, *IEEE Geosci. Remote Sens. Lett.*, *1*, 71–74, doi:10.1109/LGRS.2004.824741.

Ivanova, N., O. M. Johannessen, L. Toudal Pederson, and R. T. Tonboe (2014), Retrieval of Arctic sea ice parameters by satellite passive microwave sensors: A comparison of eleven sea ice concentration algorithms, *IEEE Trans. Geosci. Remote Sens.*, *52*, 7233–7246, doi:10.1109/TGRS.2014.2301136.

Ivanova, N., et al. (2015), Satellite passive microwave measurements of sea ice concentration: An optimal algorithm and challenges, *Cryosphere Discuss.*, *9*, 1269–1313, doi:10.5194/tcd-9-1269-2015.

Jackson, J. M., W. J. Williams, and E. C. Carmack (2012), Winter sea-ice melt in the Canada Basin, Arctic Ocean, *Geophys. Res. Lett.*, *39*, L03603, doi:10.1029/2011GL050219.
Jakobson, E., T. Vihma, T. Palo, L. Jakobson, H. Keernik, and J. Jaagus (2012), Validation of atmospheric reanalyses over the central Arctic Ocean, *Geophys. Res. Lett.*, *39*, L10802, doi:10.1029/2012GL051591.
Kay, J. E., M. M. Holland, and M. M. Jahn (2011), Inter-annual to multi-decadal Arctic sea ice extent trends in a warming world, *Geophys. Res. Lett.*, *38*, L15708, doi:10.1029/2011GL048008.
Kwok, R., A. Schweiger, D. A. Rothrock, S. Pang, and C. C. Kottmeier (1998), Sea ice motion from satellite passive microwave imagery assessed with ERS SAR and buoy motions, *J. Geophys. Res.*, *103*, 8191–8214, doi:10.1029/97JC03334.
L'Heureux, M. L., A. Kumar, G. D. Bell, M. S. Halpert, and R. W. Higgins (2008), Role of the Pacific-North American (PNA) pattern in the 2007 Arctic sea ice decline, *Geophys. Res. Lett.*, *35*, L20701, doi:10.1029/2008GL035205.
Maslanik, J. A., C. Fowler, J. Stroeve, S. Drobot, J. Zwally, D. Yi, and W. Emery (2007), A younger, thinner Arctic ice cover: Increased potential for rapid extensive sea ice loss, *Geophys. Res. Lett.*, *34*, L24501, doi:10.1029/2007/GL032043.
Maslanik, J., J. Stroeve, C. Fowler, and W. Emery (2011), Distribution and trends in Arctic sea ice age through spring 2011, *Geophys. Res. Lett.*, *38*, L13502, doi:10.1029/2011GL047735.
Matsumura, S., X. Zhang, and K. Yamazaki (2014), Summer Arctic atmospheric circulation response to spring Eurasian snow cover and its possible linkage to accelerated sea ice decrease, *J. Clim.*, *27*, 6551–6558, doi:10.1175/JCLI-D-13-00459.1.
Meier, W. N., J. A. Maslanik, and C. W. Fowler (2000), Error analysis and assimilation of remotely sensed ice motion within an Arctic sea Ice model, *J. Geophys. Res.*, *105*, 3339–3356, doi:10.1029/1999JC900268.
Notz, D., and J. Marotzke (2012), Observations reveal external driver for Arctic sea-ice retreat, *Geophys. Res. Lett.*, *39*, L08502, doi:10.1029/2012GL051094.
Ogi, M., and J. M. Wallace (2007), Summer minimum Arctic sea ice extent and the associated summer atmospheric circulation, *Geophys. Res. Lett.*, *34*, L12705, doi:10.1029/2007GL029897.
Ogi, M., I. G. Rigor, M. G. McPhee, and J. M. Wallace (2008), Summer retreat of Arctic sea ice: Role of summer winds, *Geophys. Res. Lett.*, *35*, L24701, doi:10.2029/2008GL035672.
Onarheim, I. H., T. Eldevik, M. Arthun, R. B. Ingvaldsen, and L. H. Smedstrud (2015), Skillful prediction of Barents Sea ice cover, *Geophys. Res. Lett.*, *42*, 5371–5394, doi:10.1002/2015GL064359.
Overland, J. E., J. A. Francis, E. Hanna, and M. Wang (2012), The recent shift in early summer atmospheric circulation, *Geophys. Res. Lett.*, *39*, L19804, doi:10.1029/2012GL053268.
Polyakov, I. V., et al. (2010), Arctic Ocean warming contributes to reduced polar ice cap, *J. Phys. Oceanogr.*, *40*, 2743–2756, doi:10.1175/2010JPO4339.1.
Post, E., U. S. Bhatt, C. M. Bitz, J. F. Brodie, T. L. Fulton, M. Hebblewhite, J. Kerby, S. L. Kutz, I. Stirling, and D. A. Walker (2013), Ecological consequences of sea ice decline, *Science*, *341*, 519–524, doi:10.1126/science.1235225.
Rienecker, M. M., et al. (2011), MERRA—NASA's Modern-Era Retrospective Analysis for Research and Applications, *J. Clim.*, *24*, 3624–3648, doi:10.1175/JCLI-D-00015.1.
Rigor, I. G., J. M. Wallace, and R. L. Colony (2002), Response of sea ice to the Arctic Oscillation, *J. Clim.*, *15*, 2648–2663.
Rogers, J. C. (1978), Meteorological Factors affecting interannual variability of summertime ice extent in the Beaufort Sea, *Mon. Weather Rev.*, *106*, 890–897.
Screen, J. A., I. Simmonds, and K. Keay (2011), Dramatic interannual changes of perennial Arctic sea ice linked to abnormal summer storm activity, *J. Geophys. Res.*, *116*, D15105, doi:10.1029/2011JD015847.
Serreze, M. C., and A. P. Barrett (2008), The summer cyclone maximum over the central Arctic Ocean, *J. Clim.*, *21*, 1048–1065, doi:10.1175/2007JCLI1810.1.
Serreze, M. C., and A. P. Barrett (2011), Characteristics of the Beaufort Sea high, *J. Clim.*, *24*, 159–182, doi:10.1175/2010JCL3636.1.
Serreze, M. C., and J. Stroeve (2015), Arctic sea ice trends, variability and implications for seasonal forecasting, *Phil. Trans. Royal. Soc. A*, *373*, 20140159, doi:10.1098/rsta.2014.0159.
Serreze, M. C., J. A. Maslanik, J. R. Key, R. F. Kokaly, and D. A. Robinson (1995), Diagnosis of the record minimum in Arctic sea ice area during 1990 and associated snow cover extremes, *Geophys. Res. Lett.*, *22*, 2183–2186, doi:10.1029/95GL02068.
Serreze, M. C., J. Maslanik, T. A. Scambos, F. Fetterer, J. Stroeve, K. Knowles, C. Fowler, S. Drobot, R. Barry, and T. M. Haran (2003), A record minimum Arctic sea ice extent and area in 2002, *Geophys. Res. Lett.*, *30*(3), 1110, doi:10.1029/2002GL016406.
Serreze, M. C., M. M. Holland, and J. Stroeve (2007), Perspectives on the Arctic's shrinking sea ice cover, *Science*, *315*, 1533–1536.
Serreze, M. C., A. P. Barrett, and J. Stroeve (2012), Recent changes in tropospheric water vapor over the Arctic as assessed from radiosondes and atmospheric reanalyses, *J. Geophys. Res.*, *117*, D10104, doi:10.1029/2011JD017421.
Shimada, K., T. Kamoshida, M. Itoh, S. Nishino, E. Carmack, F. A. McLaughlin, S. Zimmermann, and A. Proshutinsky (2006), Pacific inflow: Influence on catastrophic reduction of sea ice cover in the Arctic Ocean, *Geophys. Res. Lett.*, *33*, L08605, doi:10.1029/2005GL025624.
Stroeve, J. C., M. C. Serreze, F. Fetterer, T. Arbetter, W. Meier, J. Maslanik, and K. Knowles (2005), Tracking the Arctic's shrinking ice cover: Another extreme September minimum in 2004, *Geophys. Res. Lett.*, *32*, L04501, 2005, doi:10.1029/2004GL021810.
Stroeve, J. C., V. Kattsov, A. Barrett, M. Serreze, T. Pavlova, M. Holland, and W. N. Meier (2012a), Trends in Arctic sea ice extent from CMIP5, CMIP3 and observations, *Geophys. Res. Lett.*, *39*, L19502, doi:10.1029/2012GL052676.
Stroeve, J. C., M. C. Serreze, J. E. Kay, M. M. Holland, W. N. Meier, and A. P. Barrett (2012b), The Arctic's rapidly shrinking sea ice cover: A research synthesis, *Clim. Change*, *110*, 1005–1027, doi:10.1007/s10584-011-0101-1.
Stroeve, J. C., L. Hamilton, C. Bitz, and E. Blanchard-Wigglesworth (2014), Predicting September sea ice: Ensemble skill of the SEARCH sea ice outlook 2008-2013, *Geophys. Res. Lett.*, 2411–2418, doi:10.1002/2014GL059388.
Stroeve, J. C., E. Blanchard-Wrigglesworth, V. Guemas, S. Howell, F. Massonnet, and S. Tietsche (2015), *Developing User-Oriented Seasonal Ice Forecasts in a Changing Arctic*, vol. 96, *Eos Trans*., AGU, Washington, D. C., doi:10.1029/2015EO031431.
Stroeve, J., M. Serreze, S. Drobot, S. Gearheard, M. Holland, J. Maslanik, W. Meier, and T. Scambos (2008), *Arctic Sea Ice Extent Plummets in 2007*, *EOS Trans*., vol. 89, pp. 13–14, AGU, Washington, D. C.
Susskind, J., C. D. Barnet, and J. M. Blaisdell (2003), Retrieval of atmospheric and surface parameters from AIRS/AMSU/HSB data in the presence of clouds, *IEEE Trans. Geosci. Remote Sens.*, *40*, 390–409.
Susskind, J., J. M. Blaisdell, L. Iredell, and F. Keita (2011), Improved temperature sounding and quality control methodology using AIRS/AMSU data: The AIRS science team version 5 retrieval algorithm, *IEEE Trans. Geosci. Remote Sens*, *49*, 883–907.
Susskind, J., J. M. Blaisdell, and L. Iredell (2014), Improved methodology for surface and atmospheric soundings, error estimates, and quality control procedures: The atmospheric infrared sounder science team version-6 retrieval algorithm, *J. Appl. Remote Sens.*, *8*, doi:10.1117/1.JR.8.084994.

Swart, N., J. Fyfe, E. Hawkins, J. E. Kay, and A. Jahn (2015), Influence of internal variability on Arctic sea ice trends, *Nat. Clim. Change*, *5*, 86–89, doi:10.1038/nclimate2483.

Tobin, D. C., H. E. Revercomb, R. O. Knuteson, B. M. Lesht, L. L. Strow, S. E. Hannon, W. F. Feltz, L. A. Moy, E. J. Fetzer, and T. S. Cress (2006), Atmospheric radiation measurement site atmospheric state best estimates for Atmospheric Infrared Sounder temperature and water vapor retrieval validation, *J. Geophys. Res.*, *111*, D09S14, doi:10.1029/2005JD006103.

Tschudi, M., C. Fowler, J. Maskanik, and J. Stroeve (2010), Tracking the movement and changing surface characteristics of Arctic sea ice, *IEEE J. Sel. Top. Appl. Earth Obs. Remote Sens.*, doi:10.1109/JSTARS.2010.2048305.

United States Navy (2014), The United States Navy Artic Roadmap for 2014 to 2030, 38 pp. [Available at www.navy.mil/docs/USN_arctic_roadmap.pdf.]

Vinje, T., and O. Finnekasa (1986), The ice transport through Fram Strait, Report Nr. 186, Oslo, Polar Institut.

Wang, J., J. Zhang, E. Watanabe, M. Ikeda, K. Mizobata, J. E. Walsh, X. Bai, and B. Wu (2009), Is the dipole anomaly a major driver to record lows in Arctic summer sea ice extent?, *Geophys. Res. Lett.*, *36*, L05706, doi:10.1029/2008GL036706.

Woodgate, R. A., T. Weingartner, and R. Lindsay (2010), The 2007 Bering Strait oceanic heat flux and anomalous Arctic sea-ice retreat, *Geophys. Res. Lett.*, *37*, L01602, doi:10.1029/2009GL041621.

Ye, H., E. J. Fetzer, D. H. Bromwich, E. F. Fishbein, E. T. Olsen, S. L. Granger, S.-Y. Lee, L. Chen, and B. H. Lambrigsten (2007), Atmospheric total precipitable water from AIRS and ECMWF during Antarctic summer, *Geophys. Res. Lett.*, *34*, L19701, doi:10.1029/2006GL028547.

Zhang, J., R. Lindsay, A. Schweiger, and M. Steele (2013), The impacts of an intense summer cyclone on 2012 Arctic sea ice retreat, *Geophys. Res. Lett.*, *40*, 720–726, doi:10.1002/grl.50190.